Modeling of 3-Coupled-Core Fiber: Comparison Between Scalar and Vector Random Coupling Models

Ekaterina Deriushkina , Jochen Schröder , *Member, IEEE, Senior Member, OSA*, and Magnus Karlsson , *Fellow, IEEE*

Abstract—Simple, fast and accurate channel models can assist not only in a process of manufacturing of novel multi-core fibers, but also in a communication link design, providing a convenient way to investigate different properties of fibers that could be appealing for transmission. Models for coupled-core fibers are in a great demand since this type of the fiber provides advantages for data transmission, e.g. by reducing the effects of modal dispersion and fiber nonlinearity. In this work we present a comparative study of key features in a three coupled-core fiber (3CCF) for scalar and vector random coupling models. Supermodes and their group delays in an unperturbed 3CCF with polarization mode mixing are comprehensively analyzed for the first time. It is shown that birefringence does not impact significantly the group delay values but it may affect the mode mixing. The intensity impulse response and its RMS width were then investigated in a 3CCF with perturbations and compared for two types of models. The shape of the averaged intensity impulse response is found to be very similar for two models and retained for various input polarization states, while in the absence of averaging, the shape of the impulse response strongly depends on the input state of polarization. We show that the calculated RMS widths of the intensity impulse response agree well with theoretical values, as well as between scalar and vector

Index Terms—Coupled-core fibers, random coupling, impulse response, group delay, modal dispersion.

I. INTRODUCTION

MPLEMENTATIONS of space-division multiplexing (SDM) in optical fiber transmission have attracted significant attention over the last decade due to the potential to increase data throughput by utilizing spatial modes to transmit additional information. A coupled-core fiber (CCF) is a particular type of multi-core SDM fibers characterized by a close core arrangement and strong coupling between the cores. It has been extensively used in transmission experiments [1], [2], [3], [4] and has shown promising results demonstrating an

Manuscript received 9 June 2023; revised 24 September 2023; accepted 3 October 2023. Date of publication 6 October 2023; date of current version 16 January 2024. This work was supported in part by Knut and Alice Wallenberg Foundation under Grant KAW 2018.0090 and in part by Swedish Research Council (VR) Project under Grant 2019-04078. (Corresponding author: Ekaterina Deriushkina.)

The authors are with the Department of Microtechnology and Nanoscience, Chalmers University of Technology, SE-41296 Gothenburg, Sweden (e-mail: ekader@chalmers.se; jochen.schroeder@chalmers.se; magnus.karlsson@chalmers.se).

Color versions of one or more figures in this article are available at $\frac{1}{1000}$ https://doi.org/10.1109/JLT.2023.3322634.

Digital Object Identifier 10.1109/JLT.2023.3322634

ability to transmit up to 172 Tbit/s of data [5]. Therefore, CCFs are considered to be one of the prime candidates for deployment of SDM fibers. Future engineering of transmission links with CCFs relies on accurate models that describe static and dynamic phenomena in such fibers. This is especially relevant for random mode coupling effects that contribute to the reduced accumulation of the modal dispersion (MD) or group delay spread (GDS) with fiber length [6].

Numerous models where CCFs of various core count were investigated can be categorized into deterministic static models and random coupling models. Deterministic static models are based on the assumption that the mode coupling is constant over time. These models usually apply coupled-mode theory [7] for characterising coupling effects in CCFs. This model was demonstrated in the simplest case of a two coupled-core fiber (2CCF) [8] for characterization of intermodal dispersion, with the assumption that the optical power transfer between two fiber cores can be described by the beating of the two normal modes of the composite two-core structure. Moreover, with this approach it is possible to analyze supermodes [9], [10] in an unperturbed fiber, which are the spatial eigenmodes of the superstructure. Supermodes and their propagation constants were extensively studied for different symmetry structures of CCFs in [11]. However, these models disregarded polarization of the modes and its inherent coupling. Hereinafter we refer to this case as the scalar model/case, and the case where the birefringence is taken into account will be referred as the vector model/case.

The effects of random mode coupling and group delay (GD) spread in CCFs with perturbations can be also evaluated by coupled-mode theory and were discussed in a recent work [12]. The coupled-mode equation in this case should account for random variations of coupling coefficients and the concept of the model is described by a concatenated fiber with a constant segment length and random bending curvatures given for each section [13]. Polarization mixing effects are taken into account by a rotation matrix characterizing the fiber twist, which is incorporated between each segment. The MD and its statistical properties in CCFs has been also studied using an extension of the formalism developed for polarization mode dispersion (PMD) [14]. This model was generalized to the case when mode-dependent loss (MDL) is present in the system and validated by the comparison with experimental data for a three coupled-core fiber (3CCF) [15]. The Stokes-Space analysis was also applied in [16], where it was shown that in the regime of strong mode coupling the intensity impulse response (IIR) of

0733-8724 © 2023 IEEE. Personal use is permitted, but republication/redistribution requires IEEE permission. See https://www.ieee.org/publications/rights/index.html for more information.

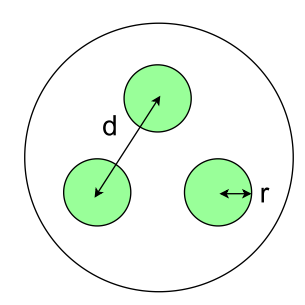


Fig. 1. Cross section of the 3CCF structure: d is a core pitch, r is a core radii.

SDM links is Gaussian and its mean-square width is given by the mean square of the MD vector of the link, confirming reported experimental observations [17]. All these works provide studies of MD where the polarization multiplexing is taken into account, but lack the comparison with the scalar case. A comparative study between the scalar and vector models can assist in analysis of possible trade-offs in design of MIMO-DSP receivers and conditions when the polarization effects have a strong impact on the investigated features or how accurately the scalar model describes the properties of a CCF.

In this work we present for the first time, to the best of our knowledge, a comparative analysis between scalar and vector models for a 3CCF. We derive for the first time an analytically tractable vector model of the supermodes, their propagation constants and GDs for an unperturbed (ideal) 3CCF, accounting for the birefringence from the presence of nearby cores. We then extend the model to account for the effects of random mode coupling and analyze the IIR as well GDs in a 3CCF by using the concatenated waveplate model. Comparisons with measured impulse responses then enable an estimate of the correlation length of the fiber. A comparison between the results in the scalar and vector cases is presented for all the studied features, which compliments Ref. [15], [16].

The article is organized as follows. In Section II we describe the supermode analysis for the scalar and vector models for an unperturbed 3CCF. The random coupling model is then presented in Section III. In Section IV we present the modeling results for the GDs in a perturbed 3CCF and analyze its IIR. Section V provides the discussion of the results and the conclusion.

II. THE UNPERTURBED 3CCF

In this section, we present the supermodes and their GDs characterization for a 3CCF with a structure depicted in Fig. 1 in the scalar case and investigate supermodes for the vector case using coupled-mode theory [7].

A. The Scalar Model

According to coupled-mode analysis, the lossless interaction between the modes of the individual cores in a 3CCF can be described by the following equation:

$$\frac{d}{dz}\vec{A} = -i\mathbf{M}\vec{A},\tag{1}$$

where $\vec{A} = (A_1 \ A_2 \ A_3)^T$ is the complex amplitude of the electrical field with D=3 components in each core and \mathbf{M} is the $D \times D$ coupling matrix. The solution then takes the form

$$\vec{A} = \mathbf{T}\vec{A_0},\tag{2}$$

where **T** is the transfer matrix of a fiber and $\vec{A_0}$ is an input amplitude vector.

In a fiber with no spatial randomness, the transfer matrix of a fiber of length L would be $\mathbf{T} = \exp(j\mathbf{M}L)$. The spatial eigenmodes, or the supermodes, can be calculated as the eigenvectors of the matrix \mathbf{T} , which in the case without randomness will be the same as the eigenvectors of the matrix \mathbf{M} :

$$\mathbf{M}(\omega) = \begin{pmatrix} \beta & c_{12} & c_{13} \\ c_{21} & \beta & c_{23} \\ c_{31} & c_{32} & \beta \end{pmatrix}$$
(3)

M contains frequency-dependent propagation constants β of the individual single mode cores (assumed to be the same) and coefficients c_{ik} describing the mode coupling from the ith core to the kth core, where i, k = 1...D. In the simplest case the coupling of ith core to the kth core is identical to the inverse coupling, so $c_{ik} = c_{ki}$ and in our calculation we further simplify it and assume that the coupling associated with all the cores is identical, so that $c_{ik} = c_{ki} = c$. The relation of the coupling coefficient c to the physical parameters of step-index cores is presented in the Appendix. Since M is Hermitian in a system with no mode-dependant loss, it can be diagonalized by a unitary matrix M:

$$\mathbf{M} = \mathbf{Y} \mathbf{\Lambda} \mathbf{Y}^{-1},\tag{4}$$

where Λ is a diagonal matrix containing the eigenvalues β_{s_k} of M:

$$\mathbf{\Lambda} = \begin{pmatrix} \beta_{s_1} & 0 & 0 \\ 0 & \beta_{s_2} & 0 \\ 0 & 0 & \beta_{s_2} \end{pmatrix}$$
 (5)

and \mathbf{Y} is a unitary matrix of the corresponding eigenvectors, which we assume to be frequency independent. Eigenvalues β_{s_k} are the frequency dependent propagation constants of the supermodes.

The propagation constants of the supermodes $\beta_{s_k}(\omega)$ can then be calculated by solving eigenvalue problem for the matrix M:

$$\beta_{s_1}(\omega) = 2c(\omega) \tag{6}$$

$$\beta_{s_2}(\omega) = \beta_{s_3}(\omega) = -c(\omega). \tag{7}$$

Note that in this calculation we neglect the propagation constant β as it is the common contribution to all eigenvalues and not important for further discussion.

The supermodes and their propagation constants $\beta_{s_k}(\omega)$ in this case are shown in Fig. 3(a). It is seen that there are three

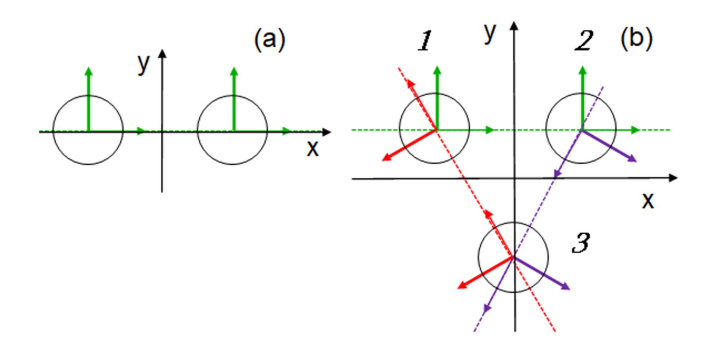


Fig. 2. Illustration of birefringence axes in (a) a 2CCF and (b) a ring-array structured 3CCF, which manifests a combination of the structure shown in (a) with its two $\pm 120^{\circ}$ -rotated 2CCF instances. The numbers 1, 2, 3 show the enumeration of the cores.

supermodes, two of which are degenerate (have the same propagation constant).

The GD is the change of the propagation constant $\beta_{s_k}(\omega)$ over the frequency ω and can be calculated as

$$\tau_k = \frac{d\beta_{s_k}(\omega)}{d\omega} L. \tag{8}$$

The GDs can also be found from the eigenvalues of the delay operator [18]:

$$\mathbf{D} = -j\mathbf{T}^{\dagger} \frac{d\mathbf{T}}{d\omega}.\tag{9}$$

Calculated GDs are shown in Fig. 3(d). Here and henceforth we use geometrical parameters of the 1.6 km 3CCF described in [19] for calculations related to the fiber. These parameters can also be found in Appendix.

Supermodes and their propagation constants for the scalar model in different CCFs were thoroughly discussed in [11] and the reader is referred to it to get more details.

B. Vector Model

In the case when the birefringence is taken into account, the coupled-mode equation describing the interaction between the modes will still have a structure of (1), however, the complex amplitude of the electrical field, \vec{A} , will contain D=6 components: $\vec{A}=(A_{1x} \ A_{1y} \ A_{2x} \ A_{2y} \ A_{3x} \ A_{3y})^T$. The coupling matrix M from (3) should be transformed to a 6×6 matrix and contain parameters of the birefringence axes, b_x and b_y . In general, this matrix can be written in the form

$$\mathbf{M}(\omega) = \begin{pmatrix} \mathbf{B_1} & \mathbf{C} & \mathbf{C} \\ \mathbf{C} & \mathbf{B_2} & \mathbf{C} \\ \mathbf{C} & \mathbf{C} & \mathbf{B_3} \end{pmatrix}$$
(10)

where $\mathbf{B_1}, \mathbf{B_2}, \mathbf{B_3}$ are 2×2 matrices describing the birefringence effects due to the presence of neighboring cores, so called form birefringence [20]. The matrices \mathbf{C} are also 2×2 and characterize the coupling between the cores. Here we as well assume that the coupling associated with all the cores is identical and orthogonal polarizations between modes do not couple, so

that C is given by

$$\mathbf{C} = \begin{pmatrix} c & 0 \\ 0 & c \end{pmatrix} \tag{11}$$

Here we neglect a birefringence in coupling coefficients for simplicity as it is a very small contribution [20].

The birefringence matrix describing birifringence effects from a neighboring core along the x-axis as in Fig. 2(a) can be expressed as

$$\mathbf{B} = \begin{pmatrix} b_x & 0\\ 0 & b_y \end{pmatrix} \tag{12}$$

and we assume for symmetry reasons that $b_y=-b_x=b$. The expression for the birefringence b is given and explained in the Appendix, but it can be observed that for typical fiber parameters, b is around 2 orders of magnitude smaller than c. Note that coupling coefficients c and the birefringence b are frequency-dependent and the group delays will be related to their frequency derivatives.

The birefringence for a 3CCF with a ring-array structure can be described using a superposition of birefringences from pairwise linear-array structures as shown in Fig. 2. As can be seen, when the cores are placed along one line, they have the same birefringence axes (2CCF case, Fig. 2(a)). However, when the third core is placed, so that the ring-array structure is formed, one has to project the birefringence from the third core to the neighboring cores (as shown in Fig. 2(b)) with the rotation matrix $\mathbf{R}(\phi)$:

$$\mathbf{R}(\phi) = \begin{pmatrix} \cos \phi & \sin \phi \\ -\sin \phi & \cos \phi \end{pmatrix} \tag{13}$$

The birefringence matrix for each core can be then calculated as the contribution from its two neighbors as

$$\mathbf{B_1} = \mathbf{B} + \mathbf{R}(-120^\circ) \cdot \mathbf{B} \cdot \mathbf{R}(120^\circ) \tag{14}$$

$$\mathbf{B_2} = \mathbf{B} + \mathbf{R}(120^\circ) \cdot \mathbf{B} \cdot \mathbf{R}(-120^\circ) \tag{15}$$

$$\mathbf{B_3} = \mathbf{R}(-120^\circ) \cdot \mathbf{B} \cdot \mathbf{R}(120^\circ) + \mathbf{R}(120^\circ) \cdot \mathbf{B} \cdot \mathbf{R}(-120^\circ)$$
(16

By plugging in B_1 , B_2 , B_3 and C from (11) to (10), the coupling matrix becomes

$$\mathbf{M}(\omega) = \begin{pmatrix} \frac{-b}{2} & \frac{\sqrt{3}b}{2} & c & 0 & c & 0\\ \frac{\sqrt{3}b}{2} & \frac{b}{2} & 0 & c & 0 & c\\ c & 0 & \frac{-b}{2} & \frac{-\sqrt{3}b}{2} & c & 0\\ 0 & c & \frac{-\sqrt{3}b}{2} & \frac{b}{2} & 0 & c\\ c & 0 & c & 0 & b & 0\\ 0 & c & 0 & c & 0 & -b \end{pmatrix}$$
(17)

The propagation constants of the supermodes are the eigenvalues of matrix \mathbf{M} and found to be

$$\beta_{s_1}(\omega) = -(c+b) \tag{18}$$

$$\beta_{s_2}(\omega) = \beta_{s_3}(\omega) = 0.5(c - \sqrt{4b^2 + 9c^2}) \approx -c - \frac{b^2}{3c}$$
 (19)

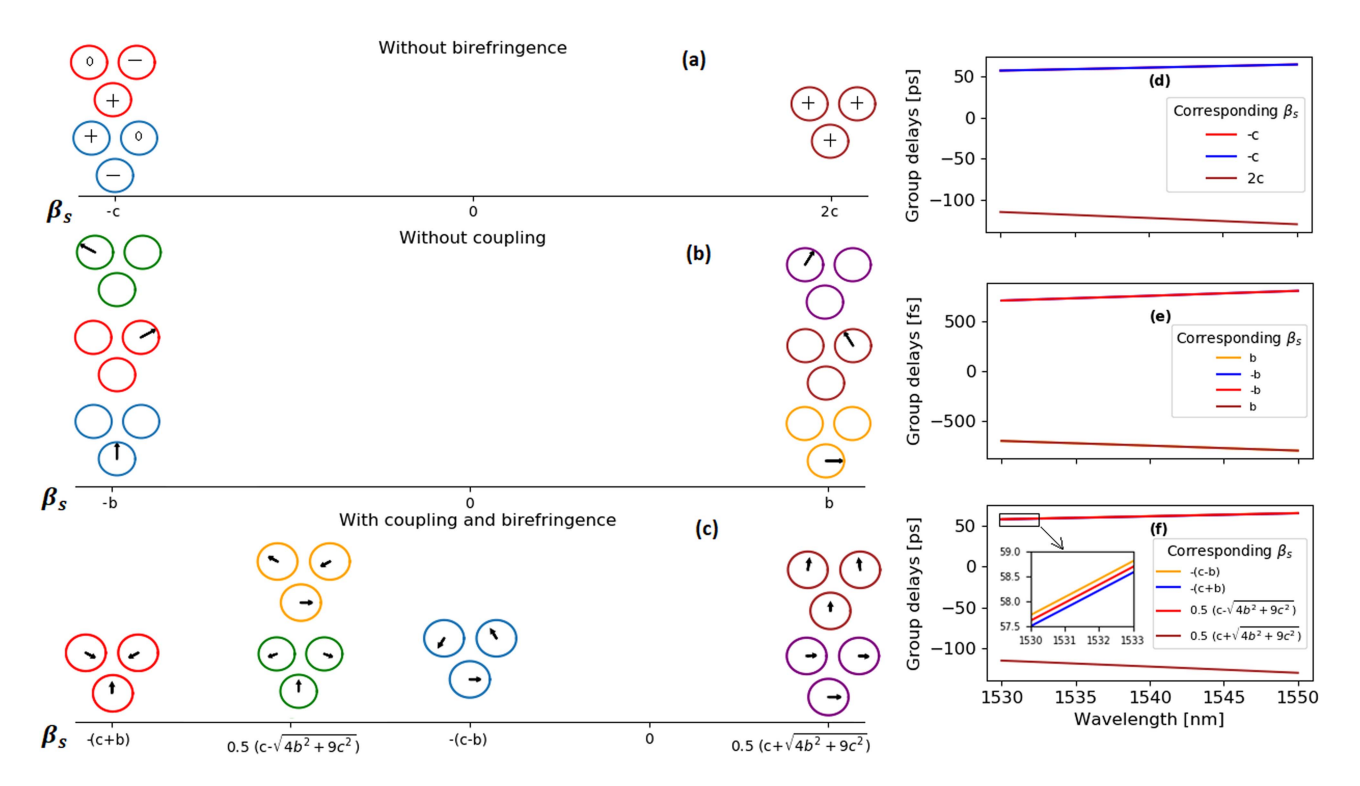


Fig. 3. Supermodes and their propagation constants in case when (a) only the coupling effects take place (scalar model), (b) only birefringence is taken into account and (c) the coupling and birefringence are taken into account (vector model). Calculated group delays for the (d) scalar model, (e) case without coupling and (f) vector model are illustrated at the right side.

$$\beta_{s_4}(\omega) = -(c-b) \tag{20}$$

$$\beta_{s_5}(\omega) = \beta_{s_6}(\omega) = 0.5(c + \sqrt{4b^2 + 9c^2}) \approx 2c + \frac{b^2}{3c}.$$
 (21)

As can be seen from Fig. 3(c), there will be 6 supermodes with 2 degenerate pairs. Note that the first and second supermodes for a 3CCF are the "TE"- and "TM"-like supermodes shown in [21] which is in good agreement with these results. Supermodes and their propagation constants in Fig. 3(b) are shown to illustrate the difference between the other two cases.

The calculated GDs are shown in Fig. 3(f). As can be seen, the GDs for the vector case are very close to those in Fig. 3(d) where the birefringence is not considered. The reason for this is that the birefringence is usually much weaker in CCFs than the coupling effects and does not impact the calculation result significantly. It should also be pointed out that this model agrees with previous works [22] in absence of birefringence.

III. RANDOM COUPLING MODEL FOR A COUPLED-CORE FIBER

The core separation and ellipticity in a realistic fiber will vary by small amounts over the length of the fiber due to manufacturing imperfections, causing small variations in the core coupling and birefringence parameters, which results in a randomized core coupling and phase delay between the modes of the coupled cores. We will model this randomness as a random unitary coupling matrix occuring periodically along the fiber. In the following we will present a theoretical description of a realistic model of such a fiber with random coupling along its

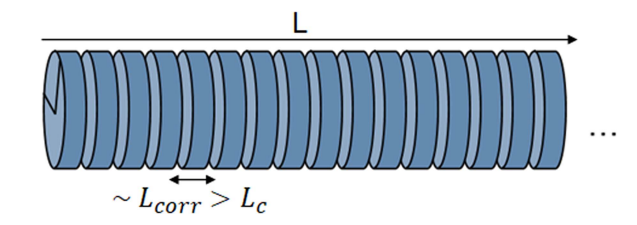


Fig. 4. Illustration of the fiber in the random coupling model: A fiber with length L is concatenated on N parts, where the length of one part should be in the range of the correlation length L_{corr} , which is larger than the coupling length L_c .

length. The equations that will be described in this section hold both in the scalar and vector cases.

We will model a random propagation in a CCF by using a concatenation rule originated from PMD calculus, which allows the determination of the PMD vector of an assembly of concatenated fiber sections when the PMD vectors of the individual sections are known [23]. Fig. 4 shows the schematic of the fiber with the total length L, which is divided into N segments with a constant segment length. The length of each section should be at least slightly longer than the correlation length L_{corr} , so that the local principal modes (PMs) in the different sections can be considered independent. This condition is analogous to the original concatenation model where short birefringent fiber segments should have constant principal states of polarization. A piece of length of a CCF is modeled with the delay matrix

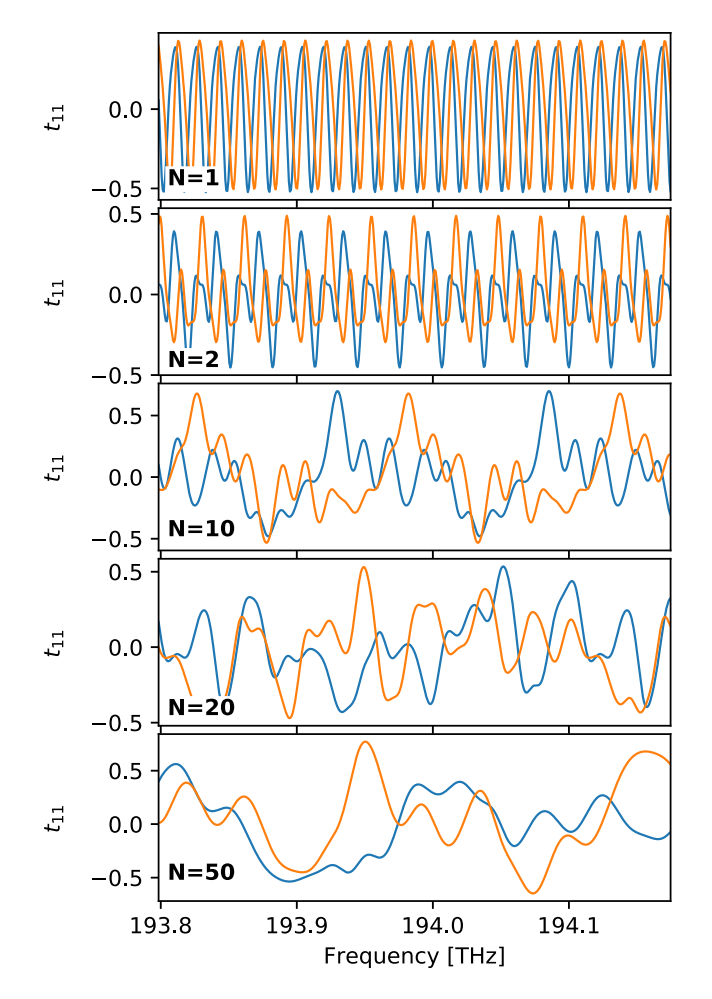


Fig. 5. Real (blue) and imaginary (orange) parts of the element t_{11} of a random transfer matrix $\mathbf{T_{tot}}$ calculated with different number of fiber concatenations N for the vector model.

 T_d :

$$\mathbf{T_d} = \exp\left(j\mathbf{M}(\omega)L_d\right),\tag{22}$$

where L_d is the element length, and $\mathbf{M}(\omega)$ is the frequency-dependent coupling matrix described previously.

Random perturbations in CCFs can be considered by introducing a random unitary matrix U in the coupled-mode equation and can be modeled in various ways [12]. As mentioned above, the randomness in real CCFs is likely a variation in core size and separations along the fiber due to manufacturing imperfections. For symmetry reasons we argue that this matrix should have the Haar distribution [24], and can be realized using QR-factorization [25].

The random coupling in a CCF can thus be modeled as a concatenated sequence of N such matrices giving a total transfer matrix $\mathbf{T_{tot}}$:

$$\mathbf{T_{tot}}(\omega) = \mathbf{T_{d,N}} \cdot \mathbf{U_N} \cdot \ldots \cdot \mathbf{T_{d,1}} \cdot \mathbf{U_1}. \tag{23}$$

The resulting matrix T_{tot} has to be unitary, as it is a product of unitary matrices.

As an example, Fig. 5 demonstrates real and imaginary parts of the element t_{11} of the 6×6 transfer function T_{tot} calculated

with different number of concatenations N for the wavelength range $\lambda=1545-1548$ nm. To compare with the 3CCF sample we have in our lab (and characterized in [19]), we have kept the total fiber length L to 1.6 km, and the length of each delay element is thus $L_d=L/N$. The other fiber parameters are given in the appendix. Since all elements have the same length, the curve is (artificially) periodic in frequency and this period is related to the inverse GDS of each element. The periodicity can simply be removed by also randomly changing the length of each element. We see that the period of fluctuations in frequency increases with N, since the GDS in each element decreases. In simulations in the next section we have used the same fiber parameters and scaling with N.

IV. ANALYSIS OF GROUP DELAYS AND IMPULSE RESPONSE IN THE 3CCF WITH RANDOM MODE COUPLING

In this section we present the results that were obtained using the random coupling model. We discuss the GDs, the total power IIR and its RMS width and compare these characteristics for the scalar and vector models.

A. Group Delays

In Section II we showed the analysis of the supermodes, which are the spatial eigenmodes of the fiber. The spatial eigenmodes enter and exit the medium in the same spatial state. However, if the random mode coupling contributes to a wavelength dependence of the transfer matrix, the spatial eigenmodes become wavelength dependent.

As was mentioned in Section II, the GDs in a fiber with the random coupling can be found by calculating eigenvalues of the delay operator \mathbf{D} , which is described by (9), where we now use \mathbf{T}_{tot} instead of \mathbf{T} .

The GDs for one realization of the transfer matrix are shown in Fig. 6 for both vector (blue) and scalar (red) models calculated for the different number of fiber concatenations N. When N=1 and N=2 it is seen that the GDs remain constant over the frequency range, while with N=10 they start to constitute random, but periodic behavior and decrease to 0 with increasing N. While the GDs converge to 0 at large N, they do not cross. As was discussed in [26], the delay operator is a random Gaussian matrix, and since the probability for such a matrix to have two identical eigenvalues is negligibly small, the GDs do not coincide. It is also notable that when N=1 the GDs calculated in case of the scalar and vector random coupling models are indistinguishable. However, with increasing N all of the delays become distinct.

Using the GDs one can calculate a fiber GDS, which can be defined in different ways. Ho and Kahn define the GDS as the difference between maximum and minimum GDs [26], while the formula derived in [27] relates the GDS to the fiber geometry and to the statistical properties of the structural fiber perturbations. We propose instead to use the average squared GDS and define it as the average of the squared eigenvalues $\tau_{\text{tot},k}$ of the delay

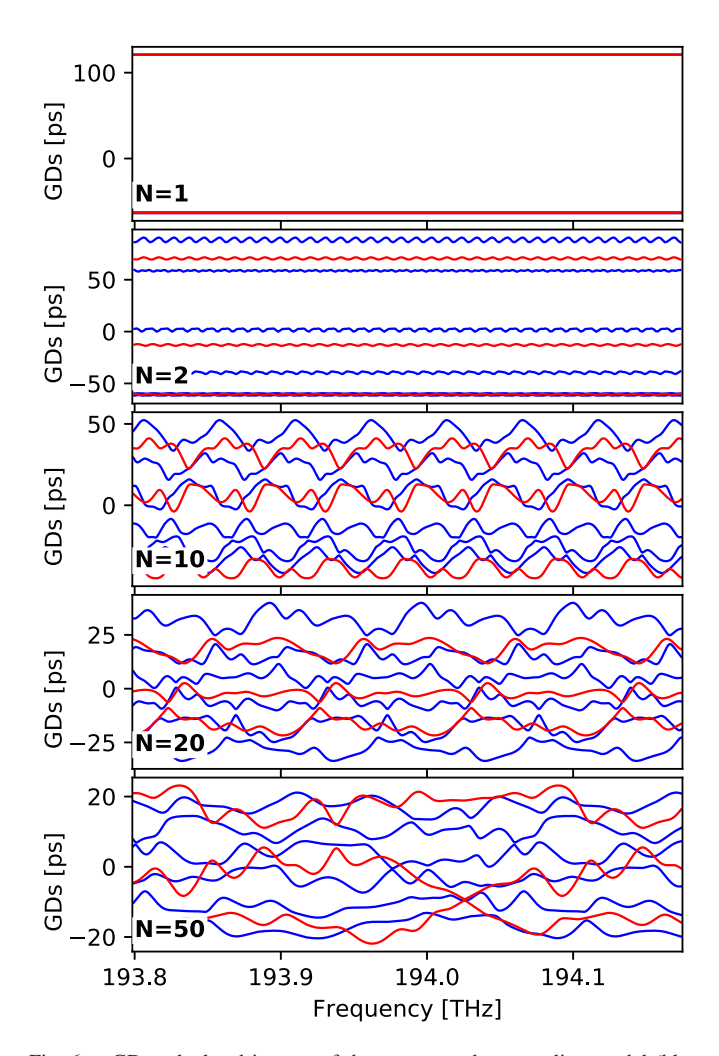


Fig. 6. GDs calculated in case of the vector random coupling model (blue curves) and scalar random coupling model (red curves) with different number of fiber concatenations N for the 1.6 km 3CCF.

operator, i.e.

$$\langle GDS^2 \rangle = \frac{1}{D} \sum_{k=1}^{D} \langle \tau_{\text{tot},k}^2 \rangle,$$
 (24)

In a concatenation of N, D-dimensional delay matrices, this can be calculated exactly as [26]

$$\langle GDS^2 \rangle = \sum_{j=1}^{N} \sum_{k=1}^{D} \frac{\langle \tau_{kj}^2 \rangle}{D},$$
 (25)

where τ_{kj} denotes the kth eigenvalue of the delay operator of element j. In our model of randomly connected unperturbed (ideal) 3CCFs of equal lengths, we have $\tau_{kj} = \tau_k$ where τ_k are the eigenvalues taken from the deterministic model given in Section II, and the squared GDS becomes

$$\langle GDS^2 \rangle = \frac{N}{D} \sum_{k=1}^{D} \tau_k^2. \tag{26}$$

The benefits of using this metric for the GDS is twofold: (i) it scales exactly linearly with fiber length, (ii) it equals the RMS

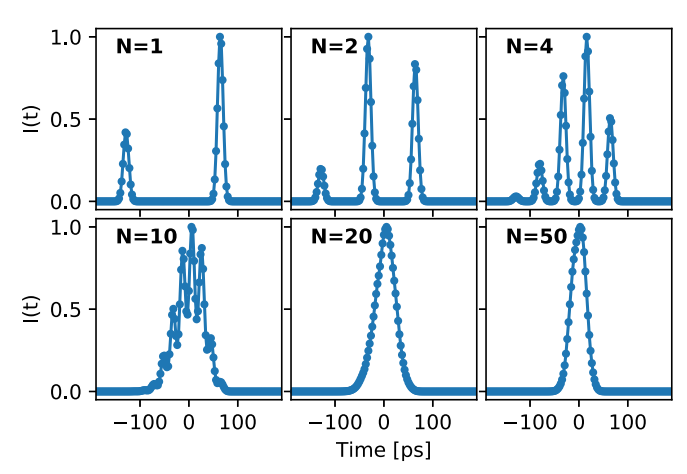


Fig. 7. Normalized total power IIR averaged over 50 realizations calculated for different number of fiber concatenations N in the scalar case.

intensity impulse response averaged over all modes (as will be shown in the next section). It also should be noted that this relation for GDS is closely related to the mean-square length of the generalized PMD vector defined in [14].

B. Impulse Response Analysis

We studied the impulse response of the 3CCF in simulations by exciting each of the core by a short Gaussian pulse and observing the received intensities in each of the cores and polarizations.

A Gaussian pulse in time domain can be expressed as

$$u(t) = \exp\left(-\frac{t^2}{2T_0^2}\right),\tag{27}$$

where t is the time coordinate and T_0 is the 1/e half-width of the pulse.

If a Gaussian pulse enters a fiber, the output complex amplitude can be found as

$$\vec{A}(t) = \mathcal{F}^{-1}[\mathbf{T_{tot}}(\omega)\vec{A_0}\mathcal{F}[u(t)]], \tag{28}$$

where $\mathcal{F}[x]$ is the Fourier transform of x. The total power IIR then can be calculated as $I(t) = \vec{A}^H(t)\vec{A}(t)$.

The total power IIR of the 3CCF calculated using the scalar model and averaged over 50 different realizations is shown in Fig. 7. We used a pulse width of $T_0 = 8$ ps and the same wavelength range as in Section III. For N = 1 there are two distinct peaks separated by 183 ps, which corresponds to GDS defined as as the difference between maximum and minimum GDs [26] and agrees well with calculation presented in Section II. As we increase the number of concatenations, there appear more peaks that move closer to the central position and the impulse response starts to be Gaussian-shaped at approximately N = 20.

The total power IIR of the 3CCF calculated using the vector model and averaged over 50 different random fiber realizations is shown in Fig. 8. Two different colors relate to the polarization of the input state. As can be seen, the input state of polarization does not affect a shape of the impulse response on average. It is also evident that these impulse responses are similar to the ones

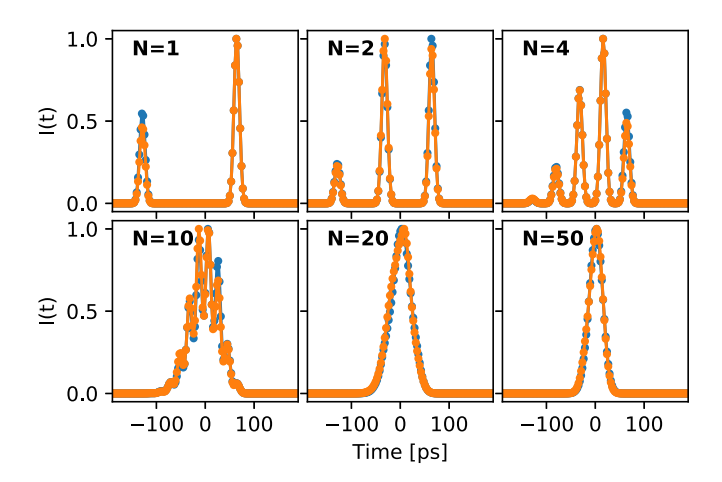


Fig. 8. Normalized total power IIR averaged over 50 realizations calculated for different number of fiber concatenations N in the vector case. Orange and blue lines are related to the instances where a Gaussian pulse is injected to x- and y-polarizations respectively.

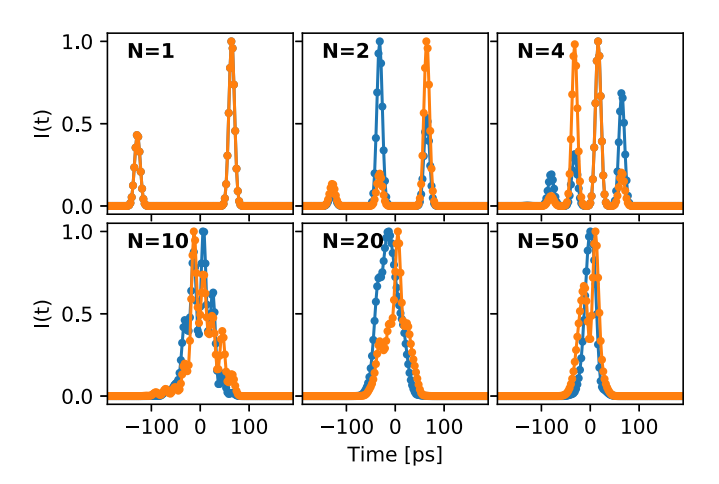


Fig. 9. Normalized total power IIR in case of 1 realization calculated for different number of fiber concatenations N in the vector case. Orange and blue lines are related to the instances where a Gaussian pulse is injected to x- and y-polarizations of core 1 respectively.

in the scalar case shown in Fig. 7. It is interesting to compare this case with a single realization, which is illustrated in Fig. 9. It is clearly seen that the polarization of the input state impacts the amplitude and the shape of the IIR. While for N=1 the impulse responses look the same for two different input conditions, the shape differs considerably for N>2.

Using the calculated total power IIRs we can obtain the RMS width as the difference between the second moment T_2 and square of the first moment T_1 :

$$T_{RMS} = \sqrt{T_2 - T_1^2},\tag{29}$$

where the first moment can be found as

$$T_1 = \frac{\int I(t) \cdot t dt}{\int I(t) dt}$$
 (30)

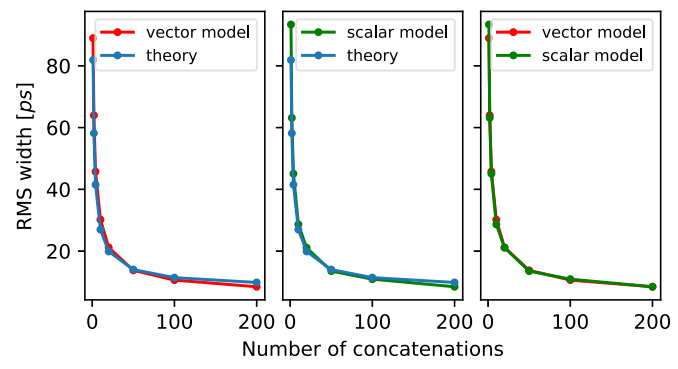


Fig. 10. Numerically calculated average RMS width of the total power IIR shown in scalar (the green curves) and vector (the red curves) cases. The blue curves show theoretical RMS widths calculated using (32).

and the second moment is

$$T_2 = \frac{\int I(t)t^2dt}{\int I(t)dt}.$$
 (31)

The estimated RMS width T_{RMS} should be also compared with ones that can be derived theoretically:

$$\langle T_{RMS}^2 \rangle_{theory} = \langle GDS^2 \rangle + T_{RMS_0}^2,$$
 (32)

where T_{RMS_0} is the RMS width of the input Gaussian pulse and τ_k are the GDs of the unperturbed fiber calculated in Section II. Here we use the same scaling as previously, keeping the total fiber length of 1.6 km constant, so $\langle GDS^2 \rangle$ is a special case of (26) and inversly proportional to N.

The dependence of the RMS width on the number of concatenations N is demonstrated in Fig. 10. Here we show three figures, where we compare the RMS widths calculated from the scalar and vector models as well as the comparison with theoretical results. It is seen that the scalar and vector models give very similar results, and at N>20 the difference becomes indistinguishable. The results also show a good agreement with theoretical estimates. We found out from the characterization experiments that the RMS widths of this 3CCF are 18.5, 18.6 and 18.9 ps for different output cores [19]. As can be noted from the Fig. 10, calculated RMS width converges to the experimental result when $N\approx30$.

V. DISCUSSION AND CONCLUSION

In this section, we discuss the results presented in Sections II, III and IV.

A. Group Delays

The GDs that we calculated in this work can be analyzed from two perspectives: a comparison between the scalar and vector model and a comparison between the GDs in an ideal fiber and in a 3CCF subjected to perturbations. As was shown in Section II, taking into account the birefringence effects does not change the GDs in an unperturbed 3CCF significantly, since in CCFs the magnitude of birefringence is much smaller than the coupling, b << c. However, in a 3CCF subject to random perturbations, the GDs become more polarization dependent and change much

more significantly. Moreover, when we increase N, they become distinct in contrast to the ideal case, when they form 2 groups. For example, in case when N=50, there is a clear difference between the GDs in the vector and scalar cases, but also the GDs related to the vector model are spaced much more than in ideal case within one group.

It should be pointed out that Fig. 6 illustrates the GDs only for one realization of the transfer matrix. The randomness of the curves that is clearly seen for cases where N=10,20,50 is averaged out when we consider many realizations and the GDs then converge to the ideal cases discussed in Section II (Fig. 3(e) and (f). By defining the net GDS from the average square sum of of the individual delays we obtain almost identical results from the scalar and vector models.

B. Impulse Response

In Section IV we demonstrated that the averaged total power IIRs calculated for the vector and scalar cases have identical shapes, as well as the RMS widths (Fig. 10). It is also demonstrated that the input state of polarization does not affect the shape significantly when the averaging takes place. On the contrary, changing the input state of polarization alters the shape of the IIRs in case of a singe realization.

As has been reported in [17], the shape of the impulse response of a 3CCF is Gaussian, which was also verified by theory and simulations in [16]. It can be noted that in our simulations the IIR's shape becomes Gaussian after N = 20.

Finally we verified that the average RMS width of the impulse response agrees well with an analytical formula exploiting the average squared GDS, defined as suggested above.

The notebooks with simulation results and calculation files within this work are accessible at [28].

APPENDIX

The coupling coefficients in matrix M can be calculated from the equation below [7]:

$$c(\omega) = \sqrt{\frac{n_1^2(\omega) - n_2^2(\omega)}{n_1^2(\omega)}} \cdot \frac{U^2}{V^3} \cdot \frac{K_0(Wd/r)}{r \cdot K_1^2(W)},$$
 (33)

where n_1 , n_2 are refractive indexes of the core and cladding accordingly, r is the core radii, d is the core pitch (diameter), V is the normalized frequency (V-parameter) and K denotes to the modified Bessel functions of the first kind. U and W can be found by solving the system of equations:

$$\begin{cases}
U \cdot K_0(W) \cdot J_1(U) = W \cdot K_1(W) \cdot J_0(U) \\
U^2 + W^2 = V^2
\end{cases} , (34)$$

where where $J_n(x)$ is the Bessel function of the first kind.

The refractive index function for the core $n_1(\omega)$ is obtained from the Sellmeier equation for fused silica [29]. The refractive index function for the cladding $n_2(\omega)$ can be calculated using the known refractive index difference Δ :

$$n_2(\omega) = n_1(\omega)\Delta. \tag{35}$$

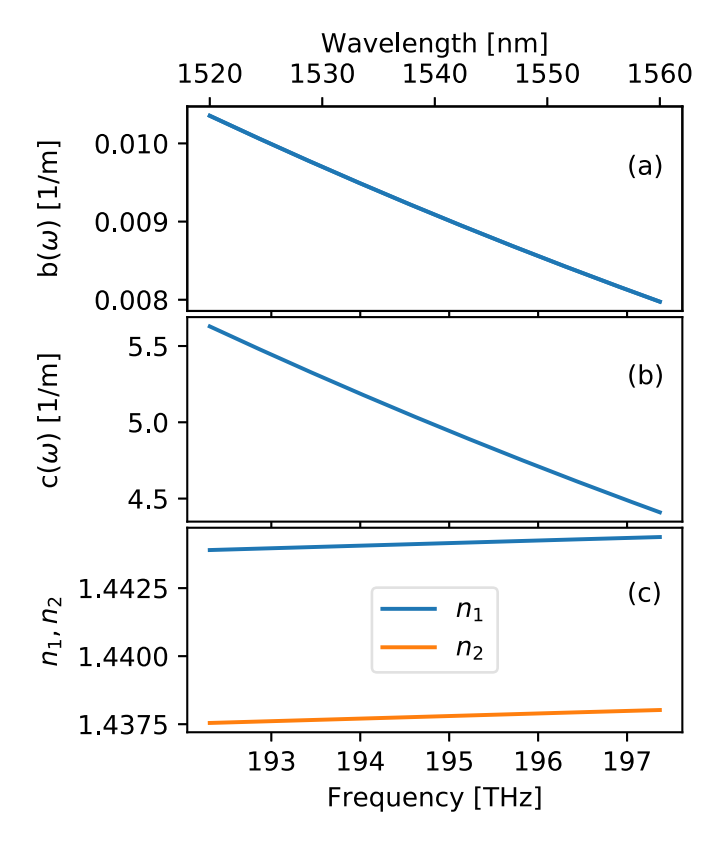


Fig. 11. Frequency/wavelength dependence of the (a) birefringence, (b) coupling coefficient and (c) refractive indices calculated for the 1.6 km 3CCF with $r=4.75~\mu\mathrm{m}$, $d=22.5~\mu\mathrm{m}$ and $\Delta=0.44\%$.

The birefringence is given by [20]

$$b(\omega) = \Delta^2 \beta \cdot \frac{4U^2 W}{V^4} \frac{K_0(W)}{K_1(W)} \times \left[\frac{I_1(W)}{K_1(W)} - \frac{I_2(W)}{K_0(W)} \right] K_2(Wd/r), \tag{36}$$

where $I_n(x)$ is the modified Bessel function of the first kind.

The frequency dependencies of the birefringence, coupling coefficients and refractive indices are depicted in Fig. 11. We used parameters of the same 3CCF [19] for calculation.

REFERENCES

- [1] R. Ryf et al., "Long-distance transmission over coupled-core multicore fiber," in *Proc. IEEE Eur. Conf. Opt. Commun.*, 2016, pp. 1–3.
- [2] R. Ryf et al., "Coupled-core transmission over 7-Core fiber," in *Proc. Opt. Fiber Commun. Conf.*, 2019, paper Th4B-3.
- [3] R.-J. Essiambre et al., "First transmission of a 12D format across three coupled spatial modes of a 3-Core coupled-core fiber at 4 bits/s/Hz," in Proc. IEEE Opt. Fiber Commun. Conf., 2020, pp. 1–3.
- [4] S. Beppu et al., "Real-time transoceanic coupled 4-core fiber transmission," in *Proc. Opt. Fiber Commun. Conf.*, 2021, paper F3B-4.
- [5] G. Rademacher et al., "High capacity transmission in a coupled-core three-core multi-core fiber," *J. Lightw. Technol.*, vol. 39, no. 3, pp. 757–762, Feb. 2021.
- [6] K.-P. Ho and J. M. Kahn, "Mode Coupling and Its Impact on Spatially Multiplexed Systems," in *Optical Fiber Telecommunications*. Amsterdam, The Netherlands: Elsevier, 2013, pp. 491–568.
- [7] A. W. Snyder, "Coupled-mode theory for optical fibers," J. Opt. Soc. Amer., vol. 62, no. 11, pp. 1267–1277, Nov. 1972.

- [8] K. S. Chiang, "Intermodal dispersion in two-core optical fibers," Opt. Lett., vol. 20, no. 9, pp. 997–999, 1995.
- [9] C. Xia, N. Bai, I. Ozdur, X. Zhou, and G. Li, "Supermodes for optical transmission," *Opt. Exp.*, vol. 19, no. 17, pp. 16653–16664, 2011.
- [10] J. Zhou and H. Pu, "Analytical expressions for the crosstalk of supermodes in the tightly bounded multicore fibers," *Opt. Exp.*, vol. 30, no. 4, pp. 4833–4844, 2022.
- [11] C. Xia et al., "Supermodes in coupled multi-core waveguide structures," IEEE J. Sel. Topics Quantum Electron., vol. 22, no. 2, pp. 196–207, Mar./Apr. 2016.
- [12] K. Saitoh, "Multi-core fiber technology for SDM: Coupling mechanisms and design," J. Lightw. Technol., vol. 40, no. 5, pp. 1527–1543, Mar. 2022.
- [13] T. Fujisawa and K. Saitoh, "Group delay spread analysis of strongly coupled 3-core fibers: An effect of bending and twisting," *Opt. Exp.*, vol. 24, no. 9, pp. 9583–9591, May 2016.
- [14] C. Antonelli, A. Mecozzi, M. Shtaif, and P. J. Winzer, "Stokes-space analysis of modal dispersion in fibers with multiple mode transmission," *Opt. Exp.*, vol. 20, no. 11, pp. 11718–11733, May 2012.
- [15] C. Antonelli, A. Mecozzi, M. Shtaif, N. K. Fontaine, H. Chen, and R. Ryf, "Stokes-space analysis of modal dispersion of SDM fibers with modedependent loss: Theory and experiments," *J. Lightw. Technol.*, vol. 38, no. 7, pp. 1668–1677, Apr. 2020.
- [16] A. Mecozzi, C. Antonelli, and M. Shtaif, "Intensity impulse response of SDM links," *Opt. Exp.*, vol. 23, no. 5, pp. 5738–5743, Mar. 2015.
- [17] R. Ryf et al., "Space-division multiplexed transmission over 4200-km 3core microstructured fiber," in *Proc. Nat. Fiber Optic Engineers Conf.*, 2012, paper PDP5C-2.
- [18] J. P. Gordon and H. Kogelnik, "PMD fundamentals: Polarization mode dispersion in optical fibers," *Proc. Nat. Acad. Sci.*, vol. 97, no. 9, pp. 4541–4550, Apr. 2000.
- [19] E. Deriushkina et al., "Characterisation of a coupled-core fiber using dual-comb swept-wavelength interferometry," in *Proc. IEEE Eur. Conf. Opt. Commun.*, 2021, pp. 1–4.

- [20] A. Ankiewicz, A. Snyder, and X.-H. Zheng, "Coupling between parallel optical fiber cores–critical examination," *J. Lightw. Technol.*, vol. 4, no. 9, pp. 1317–1323, Sep. 1986.
- [21] R. Ryf, R.-J. Essiambre, S. Randel, M. A. Mestre, C. Schmidt, and P. J. Winzer, "Impulse response analysis of coupled-core 3-Core fibers," in *Proc. IEEE 38th Eur. Conf. Exhib. Opt. Commun.*, 2012, pp. 1–3.
- [22] C. Antonelli, A. Mecozzi, and M. Shtaif, "Delay spread in strongly coupled multi-core fibers for SDM transmission," in *Proc. Opt. Fiber Commun. Conf. Exhib.*, 2015, paper Th4C-2.
- [23] N. Gisin and J. Pellaux, "Polarization mode dispersion: Time versus frequency domains," *Opt. Commun.*, vol. 89, no. 2–4, pp. 316–323, May 1992.
- [24] N. J. Higham, Accuracy and Stability of Numerical Algorithms, 2nd ed. Philadelphia, PA, USA: SIAM, 2002, ch. 26.
- [25] N. Higham, "What is a random orthogonal matrix?," 2020. [Online]. Available: https://nhigham.com/2020/04/22/what-is-a-randomorthogonal-matrix/
- [26] K.-P. Ho and J. M. Kahn, "Statistics of group delays in multimode fiber with strong mode coupling," *J. Lightw. Technol.*, vol. 29, no. 21, pp. 3119–3128, Nov. 2011.
- [27] C. Antonelli, A. Mecozzi, and M. Shtaif, "The delay spread in fibers for SDM transmission: Dependence on fiber parameters and perturbations," *Opt. Exp.*, vol. 23, no. 3, pp. 2196–2202, Feb. 2015.
- [28] E. Deriushkina, "Notebooks and calculation files for: Modeling of the 3-Coupled-Core fiber: Comparison between scalar and vector random coupling models," 2023. [Online]. Available: https://zenodo.org/record/ 7896591
- [29] B. E. A. Saleh and M. C. Teich, Fundamentls of Photonics, 2nd ed. Hoboken, NJ, USA: Wiley, 2007.